User-Centric Clustering and Beamforming Design for Satellite-Assisted Cell-Free Networks

Yunseong Lee, Chihyun Song, Donghyun Lee, Wonjong Noh, and Sungrae Cho

***Abstract*—The exponential growth in mobile traffic has driven significant interest in cell-free networks, particularly those integrated with satellites, to support high data rates and overcome geographic limitations. In this paper, we propose a novel dynamic clustering and beamforming control that maximizes the minimum data rate in satellite-assisted user-centric cell-free networks. Specifically, we formulate a nonconvex max-min fairness problem to optimize clustering and beamforming under a user-centric cluster size and transmit power constraints. To find a solution, this problem is decomposed into two subproblems: clustering and beamforming. A modified Gale-Shapley-based user-centric clustering algorithm is proposed for the clustering subproblem, which is solved on a long-term basis using statistic channel information. The beamforming subproblem transform is transformed into a semidefinite problem using linear approximation and a linear matrix inequality. We propose a robust beamforming algorithm that considers imperfect instantaneous channel state information, solved on a short-term basis. Lastly, we analyze the computational complexity, revealing that the proposed scheme has polynomial complexity. We evaluate its performance under user mobility in satellite-assisted cell-free networks. The proposed algorithm offers significant performance gains, achieving up to a 15.15% higher minimum data rate and a 14.14% higher average data rate than zero-forcing beamforming and distance-based clustering benchmark schemes.**

I. Introduction

The sixth-generation (6G) wireless system is expected to increase traffic demands for various real-time applications compared with existing mobile networks. To support the high data rates required by the vast data traffic from various devices, multiple-input multiple-output (MIMO) technology is crucial for access points [1]. The MIMO technology enhances the network capacity by enabling APs equipped with multiple antennas to communicate with multiple users at the same time and frequency. Moreover, MIMO technology is essential for low-latency communication to handle the projected terabytes per second (TB/s) data traffic in 6G networks, which significantly exceeds 5G capabilities [2], [3]. The massive MIMO technique has garnered significant research interest [4], [5] to address high data traffic demands. This system deploys numerous antennas to enhance energy and spectral efficiency. Despite its benefits, massive MIMO faces challenges such as frequent handovers and connectivity problems.

To ensure seamless communication and quality of service (QoS), cell-free networks [6] are supposed to be suitable because they eliminate cell boundaries. In cell-free networks, distributed APs are connected to a central processing unit (CPU), which manages resource control. In contrast to traditional networks, user equipment (UE) is simultaneously served by all APs, eliminating cell areas and handovers. This setup ensures the highest signal-to-interference-plus-noise ratio (SINR) because the UE simultaneously receives signals from multiple APs. However, the channel information exchange between all APs and the CPU for transmission in the front haul increases computational complexity and power consumption. To address the issues in traditional cell-free networks, user-centric cell-free networks have been proposed [7] where a predetermined number of APs serve the UE. This approach effectively reduces overhead in the front haul; however, some edge UE may still receive low signals because of their distance from all APs or unstable channel conditions.

Satellites can be an effective means to enhance the capabilities of terrestrial networks in cell-free systems [8]–[10]. Satellites complement terrestrial networks by offering additional resources to address the increasing demand for high data rates. In addition, satellites enable connectivity in remote and underserved areas where the terrestrial infrastructure is limited or absent. Recent research has increasingly explored integrating satellite and cell-free networks to enable seamless cooperation [11]–[13]. However, resource allocation between numerous APs and satellites is challenging, especially for mobile users, requiring a technique that dynamically performs clustering and beamforming simultaneously. This work focuses on developing novel user-centric clustering and beamforming tailored to satellite-assisted cell-free networks, ensuring efficient cooperative transmission and adaptability to UE mobility.

A. Related Work

Numerous studies have been conducted on resource allocation for cell-free networks [6], [14]–[21]. Ngo *et al.* [6] proposed a cell-free networks technique with a pilot assignment and power control algorithm to improve throughput. The scheme maximizes the smallest user data rates compared with traditional small-cell networks. Moreover, Zhang *et al.* [14] suggested a resource allocation with a heuristic method as a neighborhood field optimization to increase energy efficiency and throughput. The heuristic algorithm is combined with an adaptive boosting method to determine the optimal solution to a complex hypothesis task. Vu *et al.* [15], [16] developed a framework for uplink training and resource allocation using federated learning. Their scheme minimizes channel training and execution time for learning tasks while optimizing the transmit power and processing frequency. Further, Le *et al.* [17] proposed a user clustering and beamforming scheme to optimize the transmit power of APs. Cluster center users are determined using the k-means clustering scheme, and the transmit power is allocated via an inner approximation framework. Nayebi *et al*. [18] analyzed zero-forcing precoding beamforming for cell-free networks and an approximate solution for max-min power control. Moreover, Interdonato *et al*. [19] proposed a local partial zero-forcing precoding beamforming method that provides interference cancellation gain and improves spectral efficiency. Mao *et al*. [20] proposed beamforming for sensing-only, communication-only, and joint integrated sensing and communication cases using advanced optimization techniques. The study demonstrated that cell-free systems perform better than traditional cellular systems by accounting for channel errors and target uncertainties. Zhang *et al*. [21] designed robust transmission to maximize uplink and downlink performance in cell-free networks, considering channel state information (CSI) errors. This method optimizes beamforming, power, and time allocation via an alternating optimization algorithm.

Moreover, user-centric cell-free networks [7], [22]–[29] have been extensively studied. In [22], the authors extended user-centric cell-free networks by incorporating power allocation to maximize the lower bound of the sum rate and minimum spectral efficiency. Ammar *et al*. [23] introduced distributed user scheduling and beamforming schemes with low computational complexity. A Hungarian algorithm and fractional programming were applied to optimize resource allocation. Demirhan *et al*. [24] designed a beamforming scheme for the wireless front haul between a CPU and APs to improve the end-to-end data rate. The scheme employs a suboptimal iterative solution to reduce the computing complexity for max-min fair optimization.

In contrast to traditional cell-free networks, user-centric cell-free networks are not entirely handover-free. Some studies [25], [26] have analyzed the handover rate based on the cluster size of APs, demonstrating that the handover rate is influenced by cluster size. Xiao *et al*. [27] analyzed CPU and AP handover in a hybrid AP selection method combining conventional coordinated multipoint with joint transmission for pure user-centric cooperation. The scheme demonstrated that handover rates are affected by the size of the AP in the CPU and the size of the AP set. Moreover, Kibinda *et al*. [28] introduced a handover pattern in user-centric cell-free networks and proposed a handover scheme that relies on the UE path. The scheme predicts UE mobility patterns and determines handovers. Additionally, Zaher *et al*. [29] proposed a soft handover approach using pilot association and clustering control, minimizing the handover of a master AP that assigns pilot sequences instead of other APs in a cluster.

Recently, interest has been growing regarding cooperation between cell-free networks and satellites [12], [13], [30]–[33]. For instance, Gao *et al*. [12] suggested a beamforming and power allocation scheme to maximize the sum rate using non-orthogonal multiple access for full-duplex cell-free networks with satellites. In [13], the authors analyzed the spectral efficiency of cell-free networks with satellites using zero-forcing precoding and a maximum ratio transmission scheme. Further, Abdelsadek *et al*. [30] introduced novel cell-free networks in which terrestrial users can connect to a satellite cluster. This study considered the problem of maximizing throughput and minimizing handover rates via deep learning. Riera *et al*. [31] designed a power and user allocation scheme for hybrid cell-free networks using satellites. The proposed optimization problem maximizes the minimum average data rate and is solved with a greedy algorithm. In [32], the unmanned aerial vehicle (UAV) trajectory and power allocation is optimized with a cluster of UAVs conducting joint transmission to the terrestrial users. This mixed-integer non-convex programming problem is solved using the Traveling Salesman problem. Guidotti *et al*. [33] designed federated cell-free networks consisting of a swarm of satellites and a ground system. The network improves the average spectral efficiency and reduces outages with the location information of users without requiring additional CSI.

Although integrating satellite and cell-free networks offers several advantages, some problems must be resolved. Due to the rapidly changing channel conditions caused by the mobility of satellites and users, the clusters and beamforming must be updated periodically. In particular, suitable technology that considers the correlation between clusters and beamforming is required.

B. Contributions and Organizations

In this paper, we propose a new transmission control scheme that improves the performance in satellite-assisted user-centric cell-free networks. The main contributions of this work are summarized as follows:

- We propose a joint clustering and beamforming problem for satellite-assisted user-centric cell-free networks. The problem is formulated as a nonconvex max-min problem, maximizing the minimum data rate for all UEs, considering the cluster size and power constraints of APs. The problem is divided into the subproblems of clustering and beamforming to determine the solution
- First, for the clustering subproblem, a modified Gale-Shapley (GS)-based user-centric clustering algorithm is proposed, which is solved on a long-term basis using statistical channel information.
- Second, for the beamforming subproblem, a robust beamforming algorithm that considers instantaneous imperfect channel information is proposed. The subproblem is transformed into a semidefinite problem using linear approximation and a linear matrix inequality and solved on a short-term basis.
- We analyze the computational complexity and show that the proposed scheme has polynomial complexity. The proposed scheme is compared with zero-forcing beamforming and distance-based clustering schemes under user mobility in user-centric cell-free networks. The results demonstrate that the proposed scheme enhances the minimum data rate by 15.15% and the average data rate by 14.14%. In addition, the proposed scheme provides higher performance gain as the number of APs, antennas, and UE increases.

The remainder of this paper is organized as follows. Section II presents the proposed satellite-assisted user-centric cell-free network model is presented. Next, Section III discusses

TABLE I: Research on cell-free networks using satellites

Ref.	Key concept	Performance metrics	Joint transmission	Channel	Mobility	Clustering	Beamforming
[12]	Maximizing the data rate for full-duplex	Data rate	Only TAPs	Imperfect	×	×	○
[13]	Estimating CSI	Spectral efficiency	Only TAPs	Perfect	×	×	×
[30]	Handover-aware power allocation	Spectral efficiency and service time	Only SAPs	Perfect	×	○	○
[31]	Maximizing the minimum SINR	Data rate and fairness	Only TAPs	Imperfect	×	○	○
[32]	Optimizing the trajectory and power allocation	Data rate	Only TAPs	Imperfect	×	×	○
Proposed	Maximize the minimum data rate	Data rate of all UEs and edge UEs	TAPs with a SAP	Imperfect	○	○	○

the proposed dynamic clustering and beamforming. Then, Section IV describes the performance evaluations. Finally, the conclusion is provided in Section V.

II. System model

A. Network Model

We consider user-centric satellite-assisted cell-free networks, which is shown in Fig. 1. The satellite-assisted user-centric cell-free networks consist of satellite APs (SAPs), terrestrial APs (TAPs), CPUs, terrestrial central server (TCS), and UEs. In a low earth orbit (LEO), numerous SAPs are organized via a satellite constellation, and all SAPs orbit at a constant speed. We assume the presence of a single SAP, supporting UEs with weak signal reception. The SAP is equipped with N_{s} uniform planar array antennas. The TAPs are distributed on the ground and jointly support the UEs. The TAP is equipped with N_{m} multiple antennas and the set of TAPs is denoted by $\mathcal{M}$. The TAPs and SAP provide cooperative transmission [34], sharing a common spectrum resource and resulting in interference, such as terrestrial or satellite interference. We denote the set of all TAPs and SAP as $\mathcal{J}$. In cell-free networks, the CPU coordinates the overall network operation by centralized signal processing. The CPU connects to each TAP through wired fiber optics and connects to the core network and TCS via backhaul links. For the coordination, the TCS collects complete knowledge of all channel conditions, clusters, and beamforming information. The system comprises mobile UEs, denoted by $\mathcal{U}$. Each UE is equipped with a single antenna. Each UE can be connected to at most K TAPs and receives multiple signals at the same time and frequency. Moreover, the UEs can be connected to only a single SAP s.

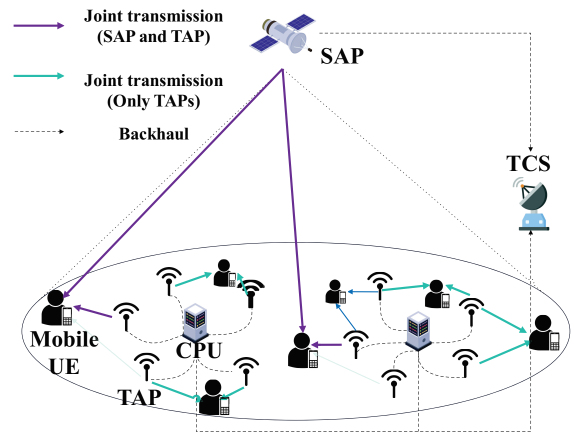

Fig. 1: Satellite-assisted user-centric cell-free networks

B. Channel Model

The channel between a TAP m and a UE u is defined as follows:

$$\mathbf{g}_{m,u} = \sqrt{\beta_{m,u}}\mathbf{h}_{m,u}, \tag{1}$$

where $\mathbf{h}_{m,u} \sim \mathcal{CN}(0,1)$ denotes the independent and identically distributed small-scale fading coefficient, and $\beta_{m,u}$ denotes the large-scale fading coefficient, expressed as in [6]

$$\beta_{m,u} = \text{PL}_{m,u} 10^{\frac{\Gamma_{m,u}\sigma_{\text{sh}}}{10}}. \tag{2}$$

In (2), $\text{PL}_{m,u}$ denotes the path loss. According to the Hata-COST231 propagation model, the path loss between the TAP and UE is given by

$$\text{PL}_{m,u} = \begin{cases} -L - 35\log_{10}(d_{m,u}) & \text{, if } d_{m,u} > d_1, \\ -L - 15\log_{10}(d_1^{1.5} d_{m,u}^2) & \text{, if } d_0 < d_{m,u} \leq d_1, \\ -L - 15\log_{10}(d_1^{1.5} d_0^2) & \text{, otherwise,} \end{cases} \tag{3}$$

where $d_{m,u}$ represents the distance between AP m and UE u, with d_0 and d_1 representing the breakpoint distances in the path loss model. The variable L can be calculated as follows:

$$\begin{aligned} L = {} & 46.3 + 33.9\log_{10}(f) - 13.82\log_{10}(h_m) \\ & - (1.11\log_{10}(f) - 0.7)h_u + (1.56\log_{10}(f) - 0.8), \end{aligned} \tag{4}$$

where f, h_m, and h_u denote the carrier frequency, TAP, and UE antenna heights, respectively. According to [35], the shadow-fading coefficient $\Gamma_{m,u}$ with two random variables components is

$$\Gamma_{m,u} = \sqrt{\eta}\epsilon_m + \sqrt{1-\eta}\epsilon_u, m \in \mathcal{M}, u \in \mathcal{U}, \tag{5}$$

where $0 \leq \eta \leq 1$ denotes a weight parameter, and $\epsilon_m \sim \mathcal{CN}(0,1)$ and $\epsilon_u \sim \mathcal{CN}(0,1)$ are independent random variables. Lastly, σ_{sh} denotes the standard deviation for shadow fading.

In practice, the UE mobility significantly affects the terrestrial channel and system performance, as noted in [36], [37]. Consequently, we consider channel realization, which includes the Doppler shift and temporal correlation for analyzing the impact of the UE mobility. As in [38], [39], the channel between the TAP m and UE u can be expressed as

$$\mathbf{g}_{m,u} = \varphi_u \breve{\mathbf{g}}_{m,u} + \sqrt{1-\varphi_u^2}\mathbf{z}_{m,u}, \tag{6}$$

where $\breve{\mathbf{g}}_{m,u}$ presents the previous the terrestrial channel state and $\mathbf{z}_{m,u} \sim \mathcal{CN}(0, \beta_{m,u})$ denotes the innovation component vector. The temporal correlation coefficient is given by

$$\varphi_u = J_0(2\pi\zeta_{D,u}T_s), \tag{7}$$

where $J_0(\cdot)$ is the zeroth-order Bessel function of the first kind, $\zeta_{D,u} = (\upsilon_u f)/c$ denotes the maximum Doppler shift for the UE, while υ_u and c denote the velocity of UE u and the speed of light, and T_s is the sampling time.

Since the high altitude of satellites ensures a strong line-of-sight (LoS) link, while non-line-of-sight (NLoS) effects are relatively weak due to the large distance and limited reflectors in the environment, non-shadowed Rician fading models are suitable for satellite communication [40], [41]. Therefore, we apply the non-shadowed Rician fading channel model and the channel between the SAP s and UE u is expressed as

$$\mathbf{g}_{s,u} = \sqrt{\beta_{s,u}}\Bigg(\underbrace{\sqrt{\frac{\kappa_{s,u}}{\kappa_{s,u}+1}}e^{j2\pi(t\zeta_{s,u}-f\xi_{s,u})}}_{\text{LoS}} + \underbrace{\sqrt{\frac{1}{\kappa_{s,u}+1}}l_{s,u}}_{\text{NLoS}}\Bigg)\mathbf{v}_{s,u}, \tag{8}$$

where $\kappa_{s,u}$ represents the Rician factor, $j=\sqrt{-1}$, $\zeta_{s,u}$ denotes the Doppler frequency shift, $\xi_{s,u}$ indicates the propagation delay, $l_{s,u} \sim \mathcal{CN}(0,1)$ denotes the independent and identically distributed small-scale fading coefficient, and $\mathbf{v}_{s,u}$ represents array response vector. The large-scale fading between the SAP s and UE u is expressed as

$$\beta_{s,u} = \mathrm{PL}_{s,u}G_sG_u, \tag{9}$$

where G_s and G_u denote the antenna gains of the SAP and ground UE. The channel in satellite-terrestrial communications experiences free space path loss, defined as follows:

$$\mathrm{PL}_{s,u} = 20\log_{10}(d_{s,u}) + 20\log_{10}(f) - 147.55, \tag{10}$$

where $d_{s,u}$ represents the distance between the SAP and UE and f denote the carrier frequency. Since the SAP is equipped with $N_\mathbf{s} = N_xN_y$ uniform planar array antennas [42], the array response vector is expressed as

$$\mathbf{v}_{s,u} = \mathbf{v}_{s,u}^x(\sin\theta_u^y\cos\theta_u^x) \otimes \mathbf{v}_{s,u}^y(\cos\theta_u^y), \tag{11}$$

where θ_u^x and θ_u^y are the space angles, and $\mathbf{v}_{s,u}^x(\cdot)$ and $\mathbf{v}_{s,u}^y(\cdot)$ are the horizontal and vertical array response vectors of the angle that can be expressed as

$$\begin{aligned}\mathbf{v}_{s,u}^x(\sin\theta_u^y\cos\theta_u^x) = \frac{1}{\sqrt{N_x}}\Big[1\ e^{-j\frac{2\pi f b_x}{c}\sin\theta_u^y\cos\theta_u^x} \\ \cdots\ e^{-j(N_x-1)\frac{2\pi f b_x}{c}\sin\theta_u^y\cos\theta_u^x}\Big]^T,\end{aligned} \tag{12}$$

$$\begin{aligned}\mathbf{v}_{s,u}^y(\cos\theta_u^y) = \frac{1}{\sqrt{N_y}}\Big[1\ e^{-j\frac{2\pi f b_y}{c}\cos\theta_u^y} \\ \cdots\ e^{-j(N_y-1)\frac{2\pi f b_y}{c}\cos\theta_u^y}\Big]^T,\end{aligned} \tag{13}$$

where b_x and b_y represent the horizontal and vertical antenna spacings. The Doppler shifts caused by the movement of the SAP can be assumed to be identical due to the relatively high altitude of the SAP [30], [43]. The Doppler shift caused by the UE movement is primarily determined by the scattering environment around the UE, allowing it to be modeled similarly to the terrestrial channel model. Similar to the terrestrial model, the channel between the SAP s and UE u including temporal correlation can be expressed as

$$\mathbf{g}_{s,u} = \varphi_u\breve{\mathbf{g}}_{s,u} + \sqrt{1-\varphi_u^2}\mathbf{z}_{s,u}, \tag{14}$$

where $\breve{\mathbf{g}}_{s,u}$ presents the previous the terrestrial channel state and $\mathbf{z}_{s,u} \sim \mathcal{CN}(0, \beta_{s,u})$ denotes the innovation component vector.

The exact CSI for $\mathbf{g}_{m,u}$ and $\mathbf{g}_{s,u}$ is challenging to determine practically due to the mobility of the UE and SAP in satellite-assisted user-centric cell-free networks. Therefore, we employ the deterministic uncertainty channel model [44], reflecting the channel errors in a specific bounded region. That is, the channels $\mathbf{g}_{m,u}$ and $\mathbf{g}_{s,u}$ are estimated as

$$\mathbf{g}_{m,u} = \hat{\mathbf{g}}_{m,u} + \Delta\mathbf{g}_{m,u}, \parallel \Delta\mathbf{g}_{m,u} \parallel \leq \varepsilon_{m,u}, \forall u, m, \tag{15}$$

$$\mathbf{g}_{s,u} = \hat{\mathbf{g}}_{s,u} + \Delta\mathbf{g}_{s,u}, \parallel \Delta\mathbf{g}_{s,u} \parallel \leq \varepsilon_{s,u}, \forall u, \tag{16}$$

where $\hat{\mathbf{g}}_{m,u}$ and $\hat{\mathbf{g}}_{s,u}$ represent measured channel information, $\Delta\mathbf{g}_{m,u}$ and $\Delta\mathbf{g}_{s,u}$ denote the estimation errors, and $\varepsilon_{m,u}$ and $\varepsilon_{s,u}$ indicate the upper bounds for the error. That is, the channel for UE u is

$$\mathbf{g}_u \triangleq \hat{\mathbf{g}}_u + \Delta\mathbf{g}_u, \parallel \Delta\mathbf{g}_u \parallel \leq \varepsilon_u, \forall u, \tag{17}$$

where,

$$\mathbf{g}_u = [\mathbf{g}_{1,u}^H, \cdots, \mathbf{g}_{M,u}^H, \mathbf{g}_{s,u}^H]^H, \tag{18}$$

$$\hat{\mathbf{g}}_u = [\hat{\mathbf{g}}_{1,u}^H, \cdots, \hat{\mathbf{g}}_{M,u}^H, \hat{\mathbf{g}}_{s,u}^H]^H, \tag{19}$$

$$\Delta\mathbf{g}_u = [\Delta\mathbf{g}_{1,u}^H, \cdots, \Delta\mathbf{g}_{M,u}^H, \Delta\mathbf{g}_{s,u}^H]^H. \tag{20}$$

C. Downlink Data Transmission

In contrast to traditional data transmission, the UE receives the same data transmitted jointly by the cooperative TAPs or SAP using the same frequency and time. Therefore, the received signal of UE u is

$$y_u = \underbrace{\sum_{m\in\mathcal{M}_u} \mathbf{g}_{m,u}^H \mathbf{w}_{m,u} x_u + \mathbf{g}_{s,u}^H \mathbf{w}_{s,u} x_u}_{\text{desired signal}} + \underbrace{\sum_{u'\in\mathcal{U}\setminus u}\sum_{m'\in\mathcal{M}_{u'}} \mathbf{g}_{m',u}^H \mathbf{w}_{m',u'} x_{u'}}_{\text{terrestrial CCI}} + \underbrace{\sum_{j\in\mathcal{U}_s} \mathbf{g}_{s,u}^H \mathbf{w}_{s,j} x_j}_{\text{satellite CCI}} + \sigma_u^2, \tag{21}$$

where $m \in \mathcal{M}_u$ denotes the indexes of the TAPs serving UE u, x_u represents the downlink data symbol, $\mathbf{w}_{m,u}$ denotes the beamforming vector of TAP m for UE u, $\mathbf{w}_{s,u}$ indicates the beamforming vector of SAP s for UE u, and σ_u represents the adaptive white Gaussian noise (AWGN). The received signal includes the signals of other UEs in the cooperative TAPs and SAP, called co-channel interference (CCI). Then, the SINR of UE u is defined as follows:

$$\delta_u = \frac{|\sum_{m\in\mathcal{M}} a_{m,u}\mathbf{g}_{m,u}^H \mathbf{w}_{m,u} + a_{s,u}\mathbf{g}_{s,u}^H \mathbf{w}_{s,u}|^2}{\sum_{u'\in\mathcal{U}'} |\sum_{m'\in\mathcal{M}} a_{m',u'}\mathbf{g}_{m',u}^H \mathbf{w}_{m',u'} + a_{s,u'}\mathbf{g}_{s,u}^H \mathbf{w}_{s,u'}|^2 + \sigma_u^2}, \tag{22}$$

where $a_{m,u}$ and $a_{s,u}$ denote the indicator value, and $\mathcal{U}' = (\mathcal{U}\setminus u)$ represents the set of UE except u. Specifically, $a_{m,u} = 1$ (or 0) if TAP m is in a cluster for UE u (or is not scheduled). Likewise, $a_{s,u} = 1$ (or 0) if SAP s is associated with UE u (or is not scheduled). Continuously, we define the clustering vector for UE u as $\mathbf{a}_u = [a_{1,u}, \cdots, a_{M,u}, a_{s,u}]$. To improve SINR, successive interference cancellation is applied to the system. According to the SINR, the data rate for UE u is defined as

$$R_u = \log_2(1 + \delta_u). \tag{23}$$

D. Problem Formulations

We formulate a user-centric clustering and beamforming problem that can be optimized for a given cluster size and power constraint. The TCS conducts clustering and beamforming in the proposed system and shares this information with the CPUs. For a concise presentation, the beamforming between TAPs and SAP for UE u is translated as

$$\mathbf{w}_u = [\mathbf{w}_{1,u}^H, \cdots, \mathbf{w}_{M,u}^H, \mathbf{w}_{s,u}^H]^H. \tag{24}$$

We define the beamforming set for APs as $\mathbf{W} = \{\mathbf{w}_u \mid u \in \mathcal{U}\}$ and the cluster for all UEs as $\mathbf{C} = \{\mathbf{a}_u \mid u \in \mathcal{U}\}$. In this study, the optimization problem to maximize the minimum data rate is formulated as

$$\begin{aligned}
(\mathbf{P}_0) \quad & \max_{\mathbf{C},\mathbf{W}} \min_{\forall u\in\mathcal{U}} \quad R_u && \text{(25a)}\\
\text{s.t.} \quad & \sum_{u\in\mathcal{U}_m} \| \mathbf{w}_{m,u} \|^2 \le P_{\max}^{\text{TAP}}, \quad \forall m \in \mathcal{M}, && \text{(25b)}\\
& \sum_{u\in\mathcal{U}_s} \| \mathbf{w}_{s,u} \|^2 \le P_{\max}^{\text{SAP}}, && \text{(25c)}\\
& \sum_{m\in\mathcal{M}} a_{m,u} = K, \quad \forall u \in \mathcal{U} && \text{(25d)}\\
& \sum_{u\in\mathcal{U}} a_{s,u} \le N_{\text{s}}, && \text{(25e)}\\
& \sum_{u\in\mathcal{U}} a_{m,u} \le N_{\text{m}}, \quad \forall m \in \mathcal{M}, && \text{(25f)}\\
& a_{m,u} = \{0, 1\}, \quad \forall u \in \mathcal{U}, \forall m \in \mathcal{M}. && \text{(25g)}\\
& \| \Delta\mathbf{g}_u \| \le \varepsilon_u, \quad \forall u. && \text{(25h)}
\end{aligned}$$

In (25b) and (25c), $\| \mathbf{w}_{m,u} \|^2 = \text{Tr}(\mathbf{w}_{m,u}\mathbf{w}_{m,u}^H)$ and $\| \mathbf{w}_{s,u} \|^2 = \text{Tr}(\mathbf{w}_{s,u}\mathbf{w}_{s,u}^H)$ denote the transmission power of TAP m and SAP s, respectively. The constraints (25b) and (25c) denote that all TAPs and the SAP have the maximum transmit power, $P_{\max}^{\text{TAP}}$ and $P_{\max}^{\text{SAP}}$, respectively. Moreover, (25d) indicates that each UE should be connected to K TAPs, and (25e) and (25f) restrict the maximum number of UEs to which TAP and SAP can connect. The problem ($\mathbf{P}_0$) is a non-convex problem with NP-complexity, making it challenging to determine a solution. Therefore, the following section decomposes the problem and proposes solutions for each subproblem.

III. Proposed Dynamic Clustering and Beamforming Control

In this section, we will decompose the problem ($\mathbf{P}_0$) into clustering and beamforming subproblems and develop solutions for each. This work suggests a modified GS-based solution for the clustering subproblem and a bisection search-based solution for the beamforming subproblem, These two subproblems are iteratively executed during the network operation, which is shown in Fig. 2 and will be elaborated in the following.

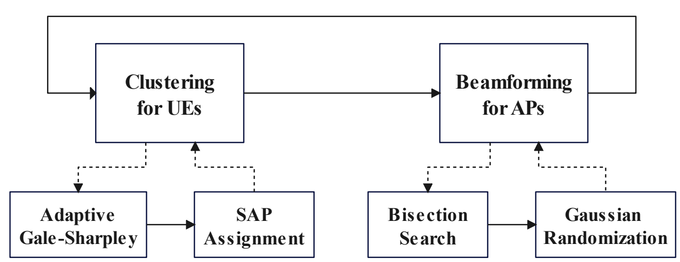

Fig. 2: Clustering and beamforming subproblems.

In practice, we assume that clustering and beamforming have different operational time-scales. Clustering is conducted on a long-term τ_c period basis, whereas beamforming is conducted on a short-term τ_b period basis, as depicted in Fig. 3.

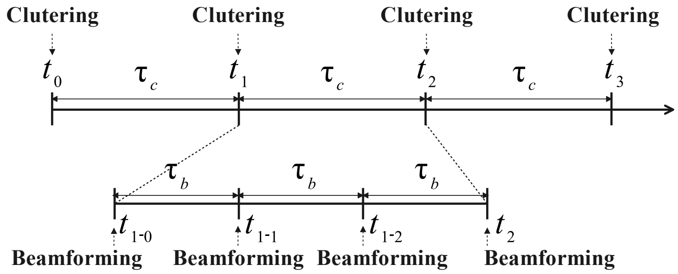

Fig. 3: Time scale for clustering and beamforming

A. Satellite-Assisted Clustering for UEs

The clustering subproblem is formulated which determine clusters that maximize the minimum data rate for a given beamforming, as follows:

$$
\begin{aligned}
(\mathbf{P_c}) \quad & \max_{\mathbf{C}} \min_{\forall u \in \mathcal{U}} \quad R_u && \text{(26a)}\\
\text{s.t.} \quad & \sum_{m \in \mathcal{M}} a_{m,u} = K, \quad \forall u \in \mathcal{U}, && \text{(26b)}\\
& \sum_{u \in \mathcal{U}} a_{s,u} \leq N_{\mathrm{s}}, && \text{(26c)}\\
& \sum_{u \in \mathcal{U}} a_{m,u} \leq N_{\mathrm{m}}, \quad \forall m \in \mathcal{M}, && \text{(26d)}\\
& a_{m,u} = \{0, 1\}, \quad \forall u \in \mathcal{U}, \quad \forall m \in \mathcal{M}. && \text{(26e)}
\end{aligned}
$$

However, calculating the data rate R_u (26a) for clustering leads to several challenges. First, at the time of clustering, the TAP and SAP do not know the beamforming for all UE, making it impossible to calculate its data rates. Second, clustering is performed on a long-term τ_c basis, while the beamforming is performed on a short-term τ_c basis. Even if the beamforming at that point is known, there is no guarantee that it will remain valid over the long-term. Therefore, as a surrogate metric, we consider effective average channel strength. The TCS is assumed to maintain the channel samples from each TAP m to each geometrical point (x_u, y_u) in the two-dimensional space to calculate the average channel strength, as follows:

$$
\mathbb{E}[\mathbf{g}_{m,u}] = \frac{1}{L_u} \sum_{v \in \mathcal{U}} \tilde{\mathbf{g}}_{m,v}^{(u)} I_u(v), \tag{27}
$$

where L_u represents the number of channel samples collected at the horizontal coordinate (x_u, y_u), $\tilde{\mathbf{g}}_{m,v}^{(u)}$ denotes the previous channel sample between TAP m and UE v when UE v is located at x_u and y_u, and $I_u(v)$ represents an indicator function given by

$$
I_u(v) = \begin{cases} 1, & \text{if UE } v \text{ was located at } (x_u, y_u), \\ 0, & \text{otherwise.} \end{cases} \tag{28}
$$

In (27), the expected channel is calculated using recent samples in the latest periods. The sum of the expected channel values associated with TAPs connected to UE u is

$$
\mathbb{E}[\phi_u] = \sum_{m \in \mathcal{M}} a_{m,u} \mathbb{E}[\mathbf{g}_{m,u}]. \tag{29}
$$

Algorithm 1 Satellite-Assisted GS-based Clustering

Input: $N_{\mathrm{m}}, N_{\mathrm{s}}, K$
Set the lower 5% of UEs as edge UEs $\mathcal{U}_e$
while $\| \mathbf{a}_u \|^2 = K, \forall u \in \mathcal{U}_e$ **do**
  Set $N_e = \min(N_{\mathrm{m}}, |\mathcal{U}_e|)$
  Edge UEs request clustering to all TAPs
  Received requests are arranged according to (27)
  Each TAP selects at most N_e edge UEs
  Each TAP replies to requests
  if $\| \mathbf{a}_u \|^2 > K, \forall u \in \mathcal{U}_e$ **then**
    The lowest TAPs are rejected
  end if
end while
while $\| \mathbf{a}_u \|^2 = K, \forall u \in \mathcal{U} \backslash \mathcal{U}_e$ **do**
  The other normal UEs request clustering to all TAPs
  Received requests are arranged according to (27)
  Set $N'_m = N_{\mathrm{m}} - \sum_{u \in \mathcal{U}_e} a_{m,u}, \quad \forall m \in \mathcal{M}$
  Each TAP selects at most N'_m UEs
  Each TAP replies to requests
  if $\| \mathbf{a}_u \|^2 > K, \forall u \in \mathcal{U}$ **then**
    The lowest TAPs are rejected
  end if
end while
The edge UEs are arranged according to (29)
The SAP sends association request to N_{s} edge UEs
The SAP connects with at the edge UEs
Output: C

That is, as a surrogate function of R_u in (26a), we use (29). Then, the clustering subproblem can be rewritten as

$$
\begin{aligned}
(\mathbf{P'_c}) \quad & \max_{\mathbf{C}} \min_{\forall u \in \mathcal{U}} \quad \mathbb{E}[\phi_u] && \text{(30a)}\\
\text{s.t.} \quad & \text{(26b), (26c), (26d), (26e).} && \text{(30b)}
\end{aligned}
$$

To solve it, we propose a GA-based clustering algorithm [45]. First, we define UE at the lowest 5% of the data rate as edge UE, and the other UE is categorized as normal UE. In the proposed algorithm, edge UEs are first associated to TAPs, and then normal UEs are associated. Thus, edge UEs first send association request messages to all TAPs for clustering. Consequently, TAPs receive multiple request messages from edge UEs, and sort them in ascending order as in (27). The TAPs select N_e edge UEs with a higher channel and inform the selected edge UEs. Afterward, for edge users with less than K TAPs from which they have been selected, the above process is repeated. Once clustering for edge UEs is completed, the same clustering procedures for normal UEs is performed. After clustering for the normal UEs, each UE calculates (29) and informs the SAP of the calculated result. Then, the SAP sorts the edge UEs in ascending order by (29), and selects the N_s edge UEs for its association. Algorithm 1 summarizes the clustering method.

B. Satellite-Assisted User-Centric Beamforming

The beamforming subproblem is formulated to determine joint beamforming from TAPs and the SAP that maximizes the minimum data rate for a given clustering as follows:

$$(\mathbf{P_b^0}) \quad \max_{\mathbf{W}} \min_{\{\Delta \mathbf{g}_u\}\forall u} \quad R_u \tag{31a}$$
$$\text{s.t.} \quad \sum_{u\in\mathcal{U}_m} \| \mathbf{w}_{m,u} \|^2 \le P_{\max}^{\mathrm{TAP}}, \quad \forall m, \tag{31b}$$
$$\sum_{u\in\mathcal{U}_s} \| \mathbf{w}_{s,u} \|^2 \le P_{\max}^{\mathrm{SAP}}, \tag{31c}$$
$$\| \Delta \mathbf{g}_u \| \le \varepsilon_u, \quad \forall u. \tag{31d}$$

The subproblem remains nonconvex; it is transformed into a standard semidefinite program (SDP) form as a convex formulation.

Defining $\{\mathbf{G}_u = \mathbf{g}_u\mathbf{g}_u^H\}_{u=1}^U$ and $\{\mathbf{W}_u = \mathbf{w}_u\mathbf{w}_u^H\}_{u=1}^U$, the data rate R_u in (31a) can be expressed using slack variables ω_u and ψ_u,

$$R_u \approx \log_2 e^{(\omega_u-\psi_u)} \tag{32}$$
$$e^{\omega_u} = \mathrm{Tr}(\mathbf{G}_u\mathbf{W}_u) + \sigma_u^2, \tag{33}$$
$$e^{\psi_u} = \sum_{u'\in\mathcal{U}\backslash u} \mathrm{Tr}(\mathbf{G}_u\mathbf{W}_{u'}) + \sigma_u^2, \tag{34}$$
$$\mathrm{Rank}(\mathbf{W}_i) = 1, i \in \mathcal{U}, \tag{35}$$

where $\mathrm{Tr}(\cdot)$ and $\mathrm{Rank}(\cdot)$ denote the trace and the rank operations of a matrix, respectively. Then, $(\mathbf{P_b^0})$ can be written with another slack variable $\mu > 0$, as follows:

$$(\mathbf{P_b^1}) \quad \max_{\mathbf{W},\Phi,\mu} \quad \mu \tag{36a}$$
$$\text{s.t.} \quad (\omega_u - \psi_u)\log_2 e \ge \mu, \quad \forall u, \tag{36b}$$
$$\mathrm{Tr}(\mathbf{G}_u\mathbf{W}_u) + \sigma_u^2 \ge e^{\omega_u}, \quad \forall u, \tag{36c}$$
$$\sum_{u'\in\mathcal{U}\backslash u} \mathrm{Tr}(\mathbf{G}_u\mathbf{W}_{u'}) + \sigma_u^2 \le e^{\psi_u}, \quad \forall u, \tag{36d}$$
$$\mathrm{Rank}(\mathbf{W}_u) = 1, \quad \forall u, \tag{36e}$$
$$\mathbf{W}_u \succeq 0. \quad \forall u, \tag{36f}$$
$$\text{(31b), (31c), (31d)}, \tag{36g}$$

where $\Phi = \{\omega_u, \psi_u\}_{u\in\mathcal{U}}$ denotes the set of slack variables. However, the transformed $(\mathbf{P_b^1})$ is still a non-convex problem due to the constraints (36c), (36d), and (36e). To address this problem, we determine the lower bound of $\mathrm{Tr}(\mathbf{G}_u\mathbf{W}_u)$ in the constraints (36c) and (36d) as

$$\begin{aligned}\mathrm{Tr}(\mathbf{G}_u\mathbf{W}_u) &= (\hat{\mathbf{g}}_u^H + \Delta\mathbf{g}_u^H)\mathbf{W}_u(\hat{\mathbf{g}}_u + \Delta\mathbf{g}_u)\\ &= (\hat{\mathbf{g}}_u^H\mathbf{W}_u + \Delta\mathbf{g}_u^H\mathbf{W}_u)(\hat{\mathbf{g}}_u + \Delta\mathbf{g}_u)\\ &= \hat{\mathbf{g}}_u^H\mathbf{W}_u\hat{\mathbf{g}}_u + 2\mathrm{Re}\{\Delta\mathbf{g}_u^H\mathbf{W}_u\hat{\mathbf{g}}_u\} + \Delta\mathbf{g}_u^H\mathbf{W}_u\Delta\mathbf{g}_u\\ &\underset{(a)}{\approx} \hat{\mathbf{g}}_u^H\mathbf{W}_u\hat{\mathbf{g}}_u + 2\mathrm{Re}\{\Delta\mathbf{g}_u^H\mathbf{W}_u\hat{\mathbf{g}}_u\}\\ &\underset{(b)}{\ge} \hat{\mathbf{g}}_u^H\mathbf{W}_u\hat{\mathbf{g}}_u + 2\varepsilon_u \| \mathbf{W}_u\hat{\mathbf{g}}_u \|,\end{aligned} \tag{37}$$

where (a) comes from that $\Delta\mathbf{g}_u^H\mathbf{W}_u\Delta\mathbf{g}_u$ is considerably small then $\hat{\mathbf{g}}_u^H\mathbf{W}_u\hat{\mathbf{g}}_u$ and $2\mathrm{Re}\{\Delta\mathbf{g}_u^H\mathbf{W}_u\hat{\mathbf{g}}_u\}$ and (b) comes from Cauchy-Schwarz inequality. Second, e^{ω_u} and e^{ψ_u} in the constraints (36c) and (36d) can be linearly approximated using the first-order Taylor series method as

$$e^{\omega_u} \approx e^{\tilde{\omega}_u}(\omega_u - \tilde{\omega}_u + 1), \tag{38}$$
$$e^{\psi_u} \approx e^{\tilde{\psi}_u}(\psi_u - \tilde{\psi}_u + 1), \tag{39}$$

where $\tilde{\omega}_u$ and $\tilde{\psi}_u$ denote the values obtained at the previous iteration in the sequential convex approximation. Then, by introducing slack variables Ω_u and Ψ_u that satisfy following,

$$\Omega_u \ge e^{\tilde{\omega}_u}(\omega_u - \tilde{\omega}_u + 1), \tag{40}$$
$$\Psi_u \le e^{\tilde{\psi}_u}(\psi_u - \tilde{\psi}_u + 1), \tag{41}$$

the problem $(\mathbf{P_b^1})$ can be rewritten as

$$(\mathbf{P_b^2}) \quad \max_{\mathbf{W},\Theta,\mu} \quad \mu \tag{42a}$$
$$\text{s.t.} \quad \hat{\mathbf{g}}_u^H\mathbf{W}_u\hat{\mathbf{g}}_u + 2\varepsilon_u \| \mathbf{W}_u\hat{\mathbf{g}}_u \| + \sigma_u^2 \ge \Omega_u, \quad \forall u, \tag{42b}$$
$$\hat{\mathbf{g}}_u^H \sum_{u'\in\mathcal{U}\backslash u} \mathbf{W}_{u'}\hat{\mathbf{g}}_u + 2\varepsilon_u \left\| \sum_{u'\in\mathcal{U}\backslash u} \mathbf{W}_{u'}\hat{\mathbf{g}}_u \right\| + \sigma_u^2 \le \Psi_u, \quad \forall u, \tag{42c}$$
$$\text{(31b), (31c), (31d), (36e), (36f), (40), (41)}, \tag{42d}$$

where $\Theta = \{\omega_u, \psi_u, \Omega_u, \Psi_u\}_{u\in\mathcal{U}}$ denotes the set of slack variables. Here, we reformulate the constraints (42b) and (42c) to linear matrix inequality form using the S-procedure [46], and drop the rank-1 constraint (36e) by the semidefinite relaxation (SDR) [47]. Then, the transformed problem $(\mathbf{P_b'})$ becomes a convex formulation as

$$(\mathbf{P_b'}) \quad \max_{\mathbf{W},\Theta,\Lambda} \quad \mu \tag{43a}$$
$$\text{s.t.} \quad \begin{bmatrix} \lambda_1\mathbf{I}_W + \mathbf{W}_u & \mathbf{W}_u\hat{\mathbf{g}}_u \\ \hat{\mathbf{g}}_u^H\mathbf{W}_u & \hat{\mathbf{g}}_u^H\mathbf{W}_u\hat{\mathbf{g}}_u - \sigma_u^2 - \lambda_1\varepsilon_u^2 - \Omega_u \end{bmatrix} \succeq 0, \quad \forall u, \tag{43b}$$
$$\begin{bmatrix} \lambda_2\mathbf{I}_W - \mathbf{V}_u & -\mathbf{V}_u\hat{\mathbf{g}}_u \\ -\hat{\mathbf{g}}_u^H\mathbf{V}_u & -\hat{\mathbf{g}}_u^H\mathbf{V}_u\hat{\mathbf{g}}_u + \sigma_u^2 - \lambda_2\varepsilon_u^2 + \Psi_u \end{bmatrix} \succeq 0, \quad \forall u, \tag{43c}$$
$$\text{(31b), (31c), (31d), (36f), (40), (41)}, \tag{43d}$$

where λ_1 and λ_2 denote auxiliary variables, $\mathbf{I}_W$ represents an identity matrix, $\mathbf{V}_u = \sum_{u'\in\mathcal{U}\backslash u}\mathbf{W}_{u'}$, and $\Lambda = \{\lambda_1, \lambda_2, \mu\}$.

To solve $(\mathbf{P_b'})$, we apply the standard convex optimization solver CVX [48] and a bisection search. In the first step, the lower bound μ_L for μ is set to 0. In addition, the maximum worst value is considered for the upper bound μ_U for μ:

$$\mu_{\max}^{\mathbf{b}} = \min_u \frac{P_{\max} \| \mathbf{g}_u \|^2}{\sigma_u^2}, \tag{44}$$

where $P_{\max}$ denotes the total transmission power of the TAPs and SAP. At each iteration, the midpoint $\mu = (\mu_L + \mu_U)/2$ is calculated as the candidate of the optimal value of μ. For the midpoint μ, if $(\mathbf{P_b'})$ has a feasible solution, μ_L is set to μ; otherwise, μ_U is set to μ. These steps are iterated until the gap between the lower bound μ_L and upper bound μ_U is less than ρ, the given precision level. If all beamforming vectors satisfy the Rank-1, eigen decomposition is conducted to obtain the optimal beamforming solutions. Otherwise, the Gaussian randomization (GR) method generates a set of candidate beamforming vectors [49].

However, the given beamforming generated using the GR method may not satisfy the power constraints (31b) and (31c). Thus, we apply the power scaling process with the given beamforming. It reduces the possibility that a particular

Algorithm 2 Satellite-Assisted User-Centric Beamforming

Input: $\mathbf{C}, P^{\text{TAP}}_{\max}, P^{\text{SAP}}_{\max}, \rho, \{\varepsilon_u\}_{u\in\mathcal{U}}$
Set $\mu_L = 0, \mu_U = \mu^{\mathbf{b}}_{\max}$
while $|\mu_U - \mu_L| > \rho$ **do**
  Set $\mu = (\mu_L + \mu_U)/2$
  Solve the problem $(\mathbf{P}'_{\mathbf{b}})$ with μ
  if $(\mathbf{P}'_{\mathbf{b}})$ is feasible **then**
    Set $\mu_L = \mu$
  else
    Set $\mu_U = \mu$
  end if
end while
if all $\text{Rank}(\mathbf{W}_j) = 1$ **then**
  Eigen decomposition to find $\mathbf{W}^\star$
else
  Generate candidate solution using GR
end if
Solve problem $\mathbf{P_s}$ using the bisection search with $\mu^{\mathbf{s}}_{\max}$
Select the set of power scaling factors P
Output: $\mathbf{W}^\star, P^\star$

user may consume too much transmission power and cause interference with other UEs. Defining the power coefficient set $P = \{p_{j,u} \mid j \in \mathcal{J}, u \in \mathcal{U}\}$, the power scaling problem is formulated as

$$(\mathbf{P_s}) \quad \max_{P,\mu} \quad \mu \tag{45a}$$

$$\text{s.t.} \quad \frac{|\sum_{m\in\mathcal{M}_u} q_{m,u} + q_{s,u}|^2}{\sum_{u'\in\mathcal{U}\backslash u} |\sum_{m'\in\mathcal{M}_{u'}} \bar{q}_{m',u'} + \bar{q}_{s,u'}|^2 + \sigma_u^2} \geq \mu \tag{45b}$$

$$\sum_{u\in\mathcal{U}_m} p_{m,u} \parallel \mathbf{w}_{m,u} \parallel^2 \leq P^{\text{TAP}}_{\max}, \quad \forall m \in \mathcal{M}, \tag{45c}$$

$$\sum_{u\in\mathcal{U}_s} p_{s,u} \parallel \mathbf{w}_{s,u} \parallel^2 \leq P^{\text{SAP}}_{\max}, \tag{45d}$$

$$p_{j,u} \geq 0, \quad \forall j \in \mathcal{J}, u \in \mathcal{U}, \tag{45e}$$

where $q_{m,u} = p_{m,u}\mathbf{g}^H_{m,u}\mathbf{w}_{m,u}$ and $\bar{q}_{m',u'} = p_{m',u'}\mathbf{g}^H_{m',u}\mathbf{w}_{m',u'}$. Similarly, the power scaling problem $(\mathbf{P_s})$ is solved by the bisection search. As in (44), we consider the maximum worst case to configure an upper bound as

$$\mu^{\mathbf{s}}_{\max} = \min_u \frac{P_{\max} |\mathbf{w}_u \mathbf{g}_u|^2}{\parallel \mathbf{w}_u \parallel^2 \sigma_u^2}. \tag{46}$$

The proposed scheme is summarized in Algorithm 2.

C. Computational Complexity

We analyze the computational complexity of the proposed clustering and beamforming, respectively. In the proposed system, we have the number of elements UM, where U and M denote the number of UEs and TAPs, respectively.

Algorithm 1 consists of GS method for the TAP clustering and SAP assignment for edge UEs. The computational complexity of the modified GS method for all UEs is $O(UM)$. In addition, the process of assigning SAP to edge UEs requires a sorting process with complexity $O(U \log U)$. That is, Algorithm 1 can be obtained by $O(UM + U \log U)$.

On the other hand, Algorithm 2 consists of a bisection search procedure to find feasible solutions and GR method. According to [50], [51], the computational complexity of bisection search is $O(M(NU)^{3.5} \log(\mu_{\max}/\rho))$ where $N = \max\{N_{\text{m}}, N_{\text{s}}\}$ is the antenna size and ρ is the solution accuracy. In addition, the GR method requires $O((NU)^2 R)$, where R is the number of random samples. Therefore, Algorithm 2 can be obtained by $O(M(NU)^{3.5} \log(\mu_{\max}/\rho) + (NU)^2 R)$.

IV. Performance Evaluation

For evaluation, we implement a MATLAB-based satellite-assisted user-centric cell-free networks simulator. We set the network size of 1000m × 1000m. The TAPs and UEs are uniformly and randomly distributed on a plane according to an independently generated independent and identically distribution, and the SAP is employed at a fixed altitude of 700 Km. We consider a Manhattan user mobility model and different UE's velocities of 1 m/s and 10 m/s [52], [53]. The simulation results are derived from an average of 200 random scenario realizations. The detailed simulation parameters are listed in Table II.

TABLE II: Simulation parameters

Parameter	Assumption
The number of UE	16
The number of TAP	32
The number of SAP	1
Carrier frequency	1.9 GHz
Bandwidth	20 MHz
Noise figure	9 dB
AP antenna height	15 m
User antenna height	1.65 m
SAP altitude	700 Km
Network size	1000 m × 1000 m
d_1, d_0	50, 10 m
$P^{\text{TAP}}_{\max}, P^{\text{SAP}}_{\max}$	200 mW, 1kW
σ_{sh}	8 dB
Mobility model	Manhattan mobility model
Average UE velocity	1m/s, 10m/s
User deployment	Uniformly distributed

The proposed scheme is compared with the following benchmark schemes under various system parameters, including cluster size, number of antenna elements, and the number of UEs.

- CBA: This is also our proposed scheme, which does not consider SAP.
- GC/ZFB [18]: This scheme employs greedy clustering (GC) and zero-forcing beamforming (ZFB) without SAP. In GC, the cluster of UE consists of the K TAPs that have strong signals.
- GC/ZFB-S [13]: This scheme employs the GC and ZFB with SAP.
- DC/ZFB: It employes the ZF-based beamforming but different clustering which is based on distance [17].
- DC/ZFB-S: This extends the fourth baseline by including SAP.

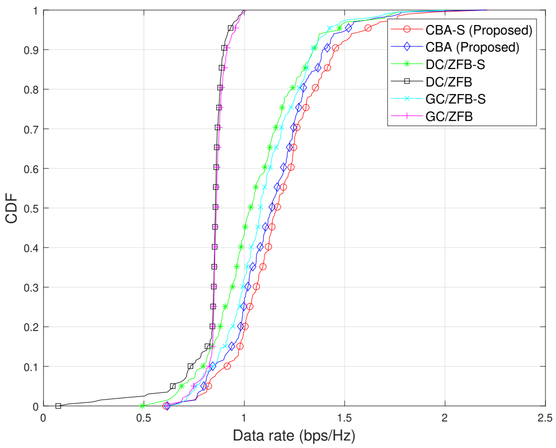

(a) $K = 2$

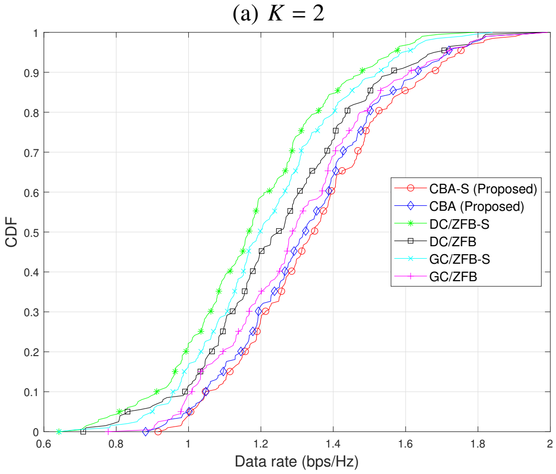

(b) $K = 4$

Fig. 4: The cumulative distribution function of minimum data rate

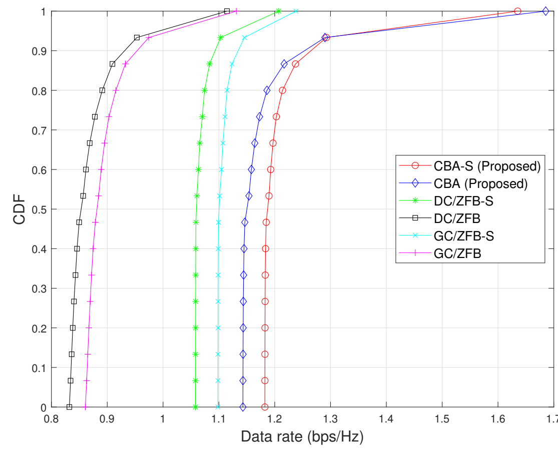

(a) $K = 2$

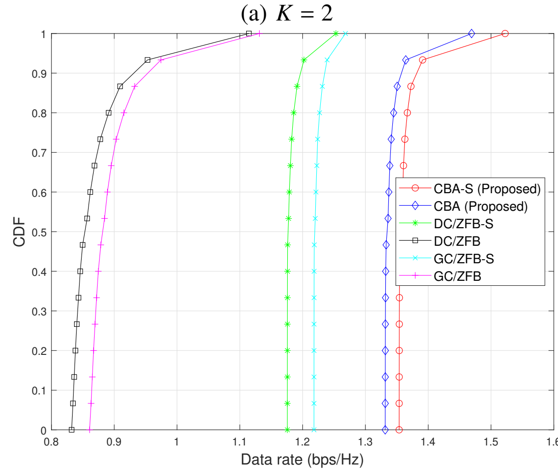

(b) $K = 4$

Fig. 5: The cumulative distribution function of average data rate

In these benchmark scenarios, users are classified into TUEs and SUEs, with SUEs associated only with SAP.

Fig. 4 compares the cumulative distribution functions (CDF) of the minimum data rate for the proposed scheme and benchmark schemes under cluster sizes $K = 2$ and $K = 4$, respectively. In this evaluation, TAP and SAP are equipped with 16 antennas, and the number of TAPs and UEs are $M = 32$ and $U = 16$. In Fig. 4(a), where the cluster size is $K = 2$, the proposed algorithm without satellite (CBA) achieves a 37.36% and 32.8% higher minimum data rate than DC/ZFB and GC/ZFB, respectively. The proposed algorithm with satellite (CBA-S) demonstrates a 15.15% and 7.67% enhanced minimum data rate over DC/ZFB-S and GC/ZFB-S, respectively. In addition, CBA-S provides a 3.44% higher minimum data rate than CBA. In Fig. 4(b), where cluster size is $K = 4$, CBA achieves a 7.72% and 3.82% enhanced minimum data rate compared with DC/ZFB and GC/ZFB, respectively, which are non-satellite benchmark schemes. In addition, CBA-S enhances the minimum data rate by 11.85% and 11.14% over DC/ZFB-S and GC/ZFB-S, respectively. Moreover, CBA-S achieves a 1.67% increased minimum data rate compared with CBA. The CBA and CBA-S demonstrate 16.49% and 14.5% enhanced performance as K increases from 2 to 4.

Fig. 5 compares the CDF of the average data rate for the proposed and benchmark schemes under cluster sizes of $K = 2$ and $K = 4$. In this evaluation, the TAP and SAP are equipped with 16 antennas, and the numbers of TAPs and UEs are $M = 32$ and $U = 16$. In Fig. 5(a), where the cluster is size $K = 2$, CBA achieves a 36.48% and 32.5% higher average data rate than DC/ZFB and GC/ZFB, respectively. Also, CBA-S shows a 14.14% and 10.04% enhanced average data rate over DC/ZFB-S and GC/ZFB-S, respectively. In addition, CBA-S achieves a 2.32% higher average data rate than CBA. In Fig. 5(b), where the cluster size is $K = 4$, CBA achieves a 53.26% and 48.79% enhanced average data rate compared with non-satellite benchmark schemes such as DC/ZFB and GC/ZFB. Further, CBA-S provides a 15.67% and 11.88% enhanced average data rate over DC/ZFB-S and GC/ZFB-S, respectively. In addition, CBA-S provides a 1.8% increased average data rate compared to CBA. As K increases from 2 to 4, CBA and CBA-s demonstrate the average data rate improvements by 12.3% and 11.73%, respectively.

Fig. 6 shows the effect of the number of TAPs on the average and edge data rates. In this evaluation, the number of UEs, number of TAP's antennas, number of SAP's antennas, and

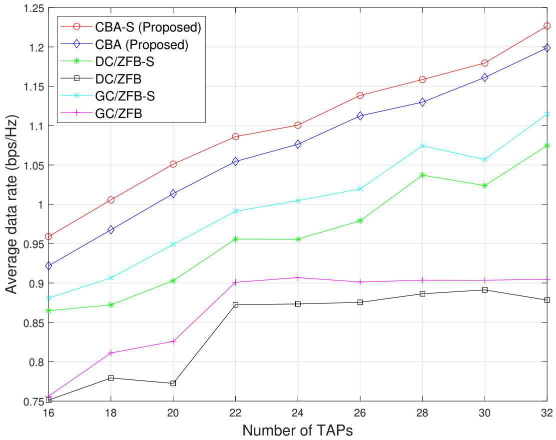

(a) All UEs

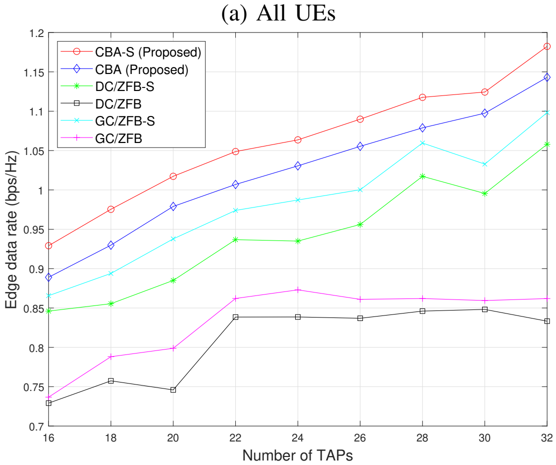

(b) Edge UEs

Fig. 6: The average data rate versus the number of TAPs

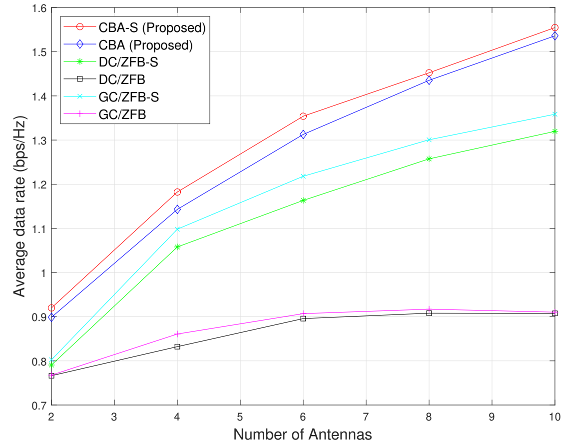

(a) All UEs

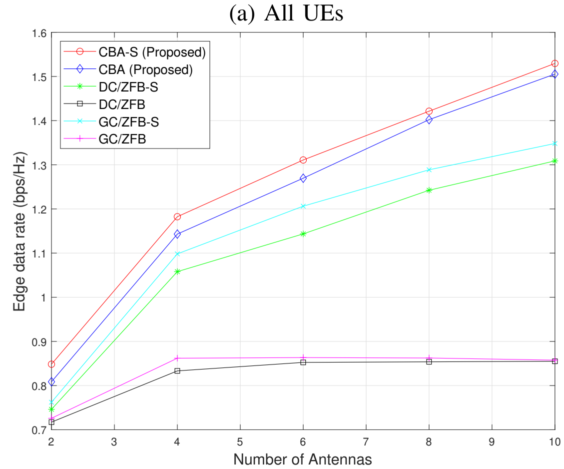

(b) Edge UEs

Fig. 7: The average data rate versus the number of antennas

cluster size for TAP are $U = 16$, $N_{\mathrm{m}} = 16$, $N_{\mathrm{s}} = 16$, and $K = 2$, respectively. Fig. 6(a) shows that CBA achieves a 27.12% and 23.31% higher average data rate than DC/ZFB and GC/ZFB, respectively. In addition, CBA-S provides a 14.3% and 10.08% enhanced average data rate over DC/ZFB-S and GC/ZFB-S. Comparing CBA-S and CBA, CBA-S provides a 2.79% higher average data rate than CBA. Fig. 6(b) shows that CBA achieves a 26.39% and 22.77% enhanced edge data rate, compared with DC/ZFB and GC/ZFB, respectively. It also shows that CBA-S provides a 12.54% and 7.09% enhanced edge data rate over DC/ZFB-S and GC/ZFB-S, respectively. Compared with CBA, it provides a 3.67% enhanced edge data rate.

Fig. 7 shows the effect of the number of antennas of the TAP on the average and edge data rates. In this evaluation, the number of UEs, number of TAPs, and cluster size are fixed at $U = 16$, $M = 32$, and $K = 2$, respectively. Fig. 7(a) shows that CBA achieves a 49.06% and 46.93% higher average data rate than DC/ZFB and GC/ZFB, respectively. Next, CBA-S demonstrates a 53.03% and 50.86% enhanced data rate over DC/ZFB-S and GC/ZFB-S, respectively. Furthermore, comparing CBA-S and CBA, CBA-S provides a 2.68% higher average data rate than CBA. Fig. 7(b) shows the average data rate for the edge UEs. First, CBA achieves a 46.78% and 45% enhancement in the average data rate of edge UEs compared with DC/ZFB and GC/ZFB, respectively. Second, the CBA-S further improves performance, with average data rate increases of 15.65% and 11.86% over DC/ZFB-S and GC/ZFB-S, respectively. Comparing CBA-S and CBA, CBA-S achieves a 2.17% higher average data rate than CBA.

Fig. 8 shows the effect of the number of UEs of the TAP on the average data rate. In this evaluation, the number of TAPs, number of antennas of TAP, number of antenna of SAP, and cluster size are fixed as $M = 32$, $N_{\mathrm{m}} = 16$, $N_{\mathrm{s}} = 16$, and $K = 2$, respectively. Fig. 8(a) shows the average data rate for all UEs. The proposed CBA shows a 10.79% and 7.89% enhanced minimum data rate over DC/ZFB and GC/ZFB, respectively. The proposed CBA-S shows a 13.28% and 10.79% enhanced minimum data rate over DC/ZFB-S and GC/ZFB-S. In addition, we can see that CBA-S provides a 0.64% higher minimum data rate than CBA. Fig. 8(b) shows the average data rate for edge UEs. The proposed CBA provides a 11.16% and 8.4% higher edge data rate than DC/ZFB and GC/ZFB, respectively. The proposed CBA-S provides a 13.85% and 11.45% higher edge data rate than DC/ZFB-S and GC/ZFB-S, respectively. In addition, comparing CBA-S and CBA, CBA-S achieves a 0.5% higher edge data rate than CBA.

Fig. 9 compares the CDF of the average data rates under perfect CSI, revealing the data rate under various imperfect

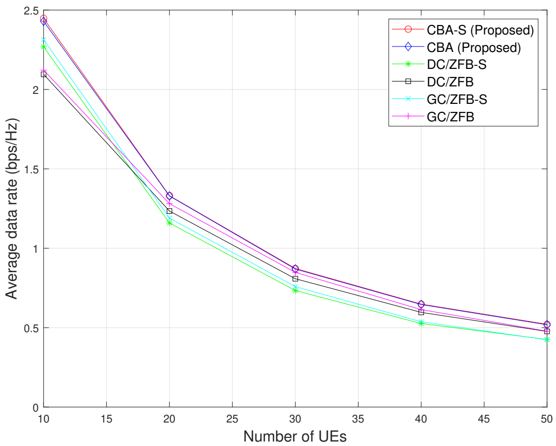

(a) All UEs

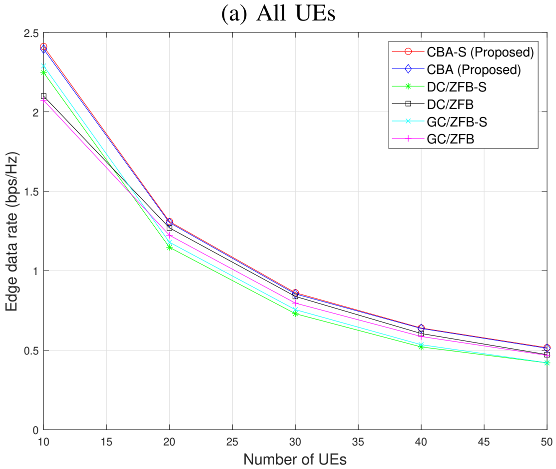

(b) Edge UEs

Fig. 8: The average data rate versus the number of UEs

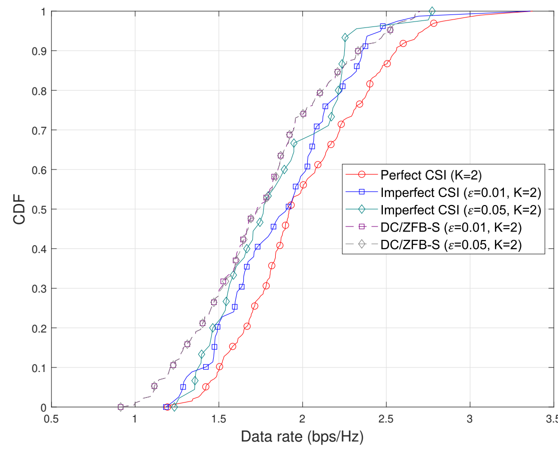

(a) $K = 2$

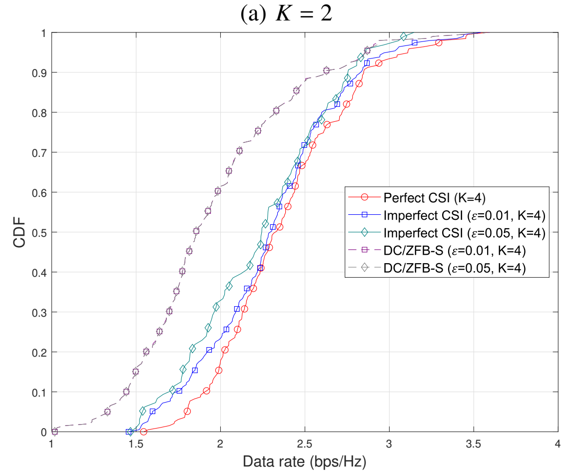

(b) $K = 4$

Fig. 9: The cumulative distribution function of data rate with imperfect channel information

CSI error bounds $\varepsilon_u = [0.01, 0.05]$ and cluster size $K = [2, 4]$, respectively. In Fig. 9(a), where the cluster size is $K = 2$, the proposed CAB-S provides a 8.12% and 4.80% higher average data rate than DC/ZFB-S with $\varepsilon = 0.01$ and $\varepsilon = 0.05$. In Fig. 9(b), where the cluster size is $K = 4$, the proposed CAB-S provides an 18.73% and 15.64% higher average data rate than DC/ZFB-S with $\varepsilon = 0.01$ and $\varepsilon = 0.05$. The results demonstrate that the proposed CBA-S maintains consistency in data rates across channel conditions while delivering superior performance.

Fig. 10 compares the CDF of the average data rates under low and high UE velocities. In this evaluation, both the TAP and SAP are equipped with 8 antennas, and the numbers of UEs and TAPs is fixed at $U = 16$ and $M = 32$, respectively. In Fig. 10(a) (cluster size $K = 2$), when the UE velocity is 1 m/s, the proposed CBA-S shows a 4.85% and 1.69% enhanced average data rate over DC/ZFB-S and GC/ZFB-S, respectively. In addition, when the UE velocity is 10 m/s, the proposed CBA-S achieves a 6.69% and 2.43% higher average data rate than DC/ZFB-S and GC/ZFB-S, respectively. In Fig. 10(b) (cluster size $K = 4$), when the UE velocity is 1 m/s, the proposed CBA-S achieves a 6.29% and 1.94% enhanced average data rate compared with DC/ZFB-S and GC/ZFB-S. Furthermore, when the UE velocity is 10 m/s, the proposed CBA-S provides a 6% and 1.89% enhanced average data rate over DC/ZFB-S and GC/ZFB-S, respectively. The results demonstrate that the proposed CBA-S provides consistenly improved performance even as the UE speed increases.

V. Conclusion

This study proposed a joint user association and beamforming control scheme that enhances the minimum data rate of UE in satellite-assisted user-centric cell-free networks. We first formulated the nonconvex max-min fairness problem that optimizes user-centric clusters and beamforming under constraints of cluster size and transmit power constraints. Then, we decomposed the objective problem into clustering and beamforming subproblems to address its non-convexity. We proposed a modified GS-based user-centric clustering algorithm for the clustering subproblem. The algorithm exploits statistical CSIc and is solved on a long-term basis. This work also designed a semi-definite programming and bisection search-based robust beamforming algorithm for the beamforming subproblem that considers imperfect CSI. The algorithm is solved on a short-term basis. Last, we confirm that the proposed control has polynomial computation complexity. The extensive simulation results reveal that the proposed

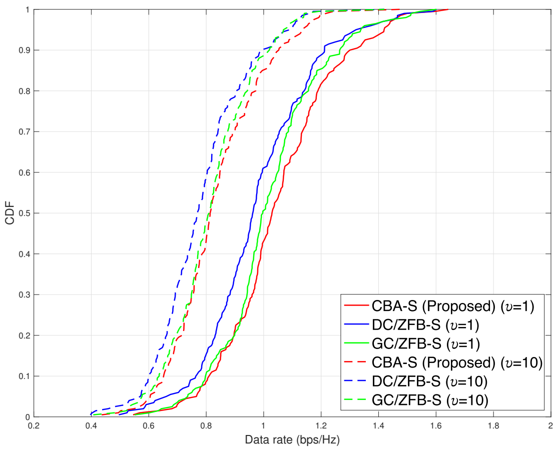

(a) $K = 2$

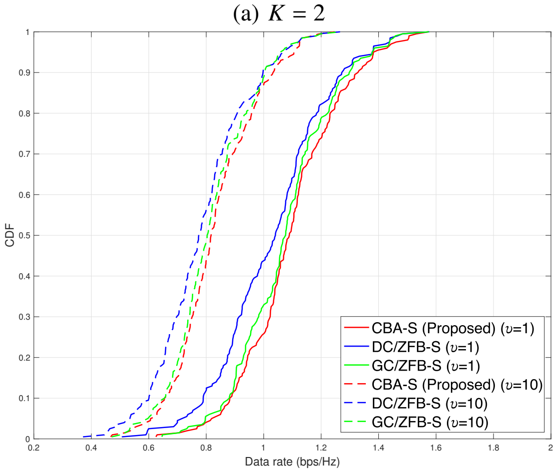

(b) $K = 4$

Fig. 10: The cumulative distribution function of data rate with different UE's velocity

control provides significant performance gains compared to ZFB and distance-based clustering based benchmark schemes under user mobility in user-centric cell-free networks.

References

[1] A. J. Paulraj, D. A. Gore, R. U. Nabar, and H. Bolcskei, "An overview of mimo communications-a key to gigabit wireless," Proceedings of the IEEE, vol. 92, no. 2, pp. 198–218, 2004.

[2] Z. Wang, J. Zhang, H. Du, D. Niyato, S. Cui, B. Ai, M. Debbah, K. B. Letaief, and H. V. Poor, "A tutorial on extremely large-scale mimo for 6g: Fundamentals, signal processing, and applications," IEEE Communications Surveys & Tutorials, 2024.

[3] K. An, Y. Sun, Z. Lin, Y. Zhu, W. Ni, N. Al-Dhahir, K.-K. Wong, and D. Niyato, "Exploiting multi-layer refracting ris-assisted receiver for hap-swipt networks," IEEE Transactions on Wireless Communications, 2024.

[4] L. Lu, G. Y. Li, A. L. Swindlehurst, A. Ashikhmin, and R. Zhang, "An overview of massive mimo: Benefits and challenges," IEEE journal of selected topics in signal processing, vol. 8, no. 5, pp. 742–758, 2014.

[5] E. G. Larsson, O. Edfors, F. Tufvesson, and T. L. Marzetta, "Massive mimo for next generation wireless systems," IEEE communications magazine, vol. 52, no. 2, pp. 186–195, 2014.

[6] H. Q. Ngo, A. Ashikhmin, H. Yang, E. G. Larsson, and T. L. Marzetta, "Cell-free massive mimo versus small cells," IEEE Transactions on Wireless Communications, vol. 16, no. 3, pp. 1834–1850, 2017.

[7] S. Buzzi and C. D'Andrea, "Cell-free massive mimo: User-centric approach," IEEE Wireless Communications Letters, vol. 6, no. 6, pp. 706–709, 2017.

[8] Z. Lin, M. Lin, B. Champagne, W.-P. Zhu, and N. Al-Dhahir, "Secrecy-energy efficient hybrid beamforming for satellite-terrestrial integrated networks," IEEE Transactions on Communications, vol. 69, no. 9, pp. 6345–6360, 2021.

[9] Z. Lin, M. Lin, T. De Cola, J.-B. Wang, W.-P. Zhu, and J. Cheng, "Supporting iot with rate-splitting multiple access in satellite and aerial-integrated networks," IEEE Internet of Things Journal, vol. 8, no. 14, pp. 11 123–11 134, 2021.

[10] S. Park, G. S. Kim, Z. Han, and J. Kim, "Quantum multi-agent reinforcement learning is all you need: Coordinated global access in integrated tn/ntn cube-satellite networks," IEEE Communications Magazine, vol. 62, no. 10, pp. 86–92, 2024.

[11] F. Riera-Palou, G. Femenias, M. Caus, M. Shaat, and A. I. Pérez-Neira, "Scalable cell-free massive mimo networks with leo satellite support," IEEE Access, vol. 10, pp. 37 557–37 571, 2022.

[12] Q. Gao, M. Jia, Q. Guo, X. Gu, and L. Hanzo, "Jointly optimized beamforming and power allocation for full-duplex cell-free noma in space-ground integrated networks," IEEE Transactions on Communications, 2023.

[13] J. Li, L. Chen, P. Zhu, D. Wang, and X. You, "Satellite-assisted cell-free massive mimo systems with multi-group multicast," Sensors, vol. 21, no. 18, p. 6222, 2021.

[14] X. Zhang, H. Qi, X. Zhang, and L. Han, "Energy-efficient resource allocation and data transmission of cell-free internet of things," IEEE Internet of Things Journal, vol. 8, no. 20, pp. 15 107–15 116, 2020.

[15] T. T. Vu, D. T. Ngo, N. H. Tran, H. Q. Ngo, M. N. Dao, and R. H. Middleton, "Cell-free massive mimo for wireless federated learning," IEEE Transactions on Wireless Communications, vol. 19, no. 10, pp. 6377–6392, 2020.

[16] T. T. Vu, D. T. Ngo, H. Q. Ngo, M. N. Dao, N. H. Tran, and R. H. Middleton, "Joint resource allocation to minimize execution time of federated learning in cell-free massive mimo," IEEE Internet of Things Journal, vol. 9, no. 21, pp. 21 736–21 750, 2022.

[17] Q. N. Le, V.-D. Nguyen, O. A. Dobre, N.-P. Nguyen, R. Zhao, and S. Chatzinotas, "Learning-assisted user clustering in cell-free massive mimo-noma networks," IEEE Transactions on Vehicular Technology, vol. 70, no. 12, pp. 12 872–12 887, 2021.

[18] E. Nayebi, A. Ashikhmin, T. L. Marzetta, H. Yang, and B. D. Rao, "Precoding and power optimization in cell-free massive mimo systems," IEEE Transactions on Wireless Communications, vol. 16, no. 7, pp. 4445–4459, 2017.

[19] G. Interdonato, M. Karlsson, E. Björnson, and E. G. Larsson, "Local partial zero-forcing precoding for cell-free massive mimo," IEEE Transactions on Wireless Communications, vol. 19, no. 7, pp. 4758–4774, 2020.

[20] W. Mao, Y. Lu, C.-Y. Chi, B. Ai, Z. Zhong, and Z. Ding, "Communication-sensing region for cell-free massive mimo isac systems," IEEE Transactions on Wireless Communications, 2024.

[21] G. Zhang, Y. Lu, M. Li, Z. Zhong, and T. Q. Quek, "Joint uplink and downlink robust transmission for cell-free networks," IEEE Transactions on Wireless Communications, 2024.

[22] S. Buzzi, C. D'Andrea, A. Zappone, and C. D'Elia, "User-centric 5g cellular networks: Resource allocation and comparison with the cell-free massive mimo approach," IEEE Transactions on Wireless Communications, vol. 19, no. 2, pp. 1250–1264, 2019.

[23] H. A. Ammar, R. Adve, S. Shahbazpanahi, G. Boudreau, and K. V. Srinivas, "Distributed resource allocation optimization for user-centric cell-free mimo networks," IEEE Transactions on Wireless Communications, vol. 21, no. 5, pp. 3099–3115, 2021.

[24] U. Demirhan and A. Alkhateeb, "Enabling cell-free massive mimo systems with wireless millimeter wave fronthaul," IEEE Transactions on Wireless Communications, 2022.

[25] W. Bao and B. Liang, "Optimizing cluster size through handoff analysis in user-centric cooperative wireless networks," IEEE Transactions on Wireless Communications, vol. 17, no. 2, pp. 766–778, 2017.

[26] E. Demarchou, C. Psomas, and I. Krikidis, "Intelligent user-centric handover scheme in ultra-dense cellular networks," in GLOBECOM 2017-2017 IEEE Global Communications Conference. IEEE, 2017, pp. 1–6.

[27] Y. Xiao, P. Mähönen, and L. Simić, "Mobility performance analysis of scalable cell-free massive mimo," arXiv preprint arXiv:2202.01488, 2022.

[28] N. M. Kibinda and X. Ge, "User-centric cooperative transmissions-enabled handover for ultra-dense networks," IEEE Transactions on Vehicular Technology, vol. 71, no. 4, pp. 4184–4197, 2022.

[29] M. Zaher, E. Björnson, and M. Petrova, “Soft handover procedures in mmwave cell-free massive mimo networks,” arXiv preprint arXiv:2209.02548, 2022.
[30] M. Y. Abdelsadek, G. K. Kurt, and H. Yanikomeroglu, “Distributed massive mimo for leo satellite networks,” IEEE Open Journal of the Communications Society, vol. 3, pp. 2162–2177, 2022.
[31] F. Riera-Palou, G. Femenias, M. Caus, M. Shaat, J. Garcia-Morales, and A. I. Pérez-Neira, “Enhancing cell-free massive mimo networks through leo satellite integration,” in 2021 IEEE Wireless Communications and Networking Conference Workshops (WCNCW). IEEE, 2021, pp. 1–7.
[32] Z. Wu and Q. Wang, “Trajectory optimization and power allocation for cell-free satellite-uav internet of things,” IEEE Access, vol. 11, pp. 203–213, 2022.
[33] A. Guidotti, A. Vanelli-Coralli, and C. Amatetti, “Federated cell-free mimo in non-terrestrial networks: Architectures and performance,” IEEE Transactions on Aerospace and Electronic Systems, 2024.
[34] X. Zhu, C. Jiang, L. Yin, L. Kuang, N. Ge, and J. Lu, “Cooperative multigroup multicast transmission in integrated terrestrial-satellite networks,” IEEE Journal on Selected Areas in Communications, vol. 36, no. 5, pp. 981–992, 2018.
[35] Z. Wang, E. K. Tameh, and A. R. Nix, “Joint shadowing process in urban peer-to-peer radio channels,” IEEE Transactions on Vehicular Technology, vol. 57, no. 1, pp. 52–64, 2008.
[36] J. Zheng, J. Zhang, E. Björnson, and B. Ai, “Impact of channel aging on cell-free massive mimo over spatially correlated channels,” IEEE Transactions on Wireless Communications, vol. 20, no. 10, pp. 6451–6466, 2021.
[37] C. D’Andrea, G. Interdonato, and S. Buzzi, “User-centric handover in mmwave cell-free massive mimo with user mobility,” in 2021 29th European Signal Processing Conference (EUSIPCO). IEEE, 2021, pp. 1–5.
[38] S. Elhoushy and W. Hamouda, “Limiting doppler shift effect on cell-free massive mimo systems: A stochastic geometry approach,” IEEE Transactions on Wireless Communications, vol. 20, no. 9, pp. 5656–5671, 2021.
[39] H. Fang, H. Hu, Y. Zhang, X. Qiao, L. Yang, and H. Zhu, “Achievable rate analysis and power optimization for cell-free massive mimo urllc systems over aging and correlated channels,” IEEE Internet of Things Journal, 2024.
[40] S. Kim, J. Wu, B. Shim, and M. Z. Win, “Cell-free massive non-terrestrial networks,” IEEE Journal on Selected Areas in Communications, 2024.
[41] L. You, K.-X. Li, J. Wang, X. Gao, X.-G. Xia, and B. Ottersten, “Massive mimo transmission for leo satellite communications,” IEEE Journal on Selected Areas in Communications, vol. 38, no. 8, pp. 1851–1865, 2020.
[42] K.-X. Li, X. Gao, and X.-G. Xia, “Channel estimation for leo satellite massive mimo ofdm communications,” IEEE Transactions on Wireless Communications, vol. 22, no. 11, pp. 7537–7550, 2023.
[43] E. G. Peters and C. R. Benson, “A doppler correcting software defined radio receiver design for satellite communications,” IEEE Aerospace and Electronic Systems Magazine, vol. 35, no. 2, pp. 38–48, 2020.
[44] Y. Lu, K. Xiong, P. Fan, Z. Zhong, and K. B. Letaief, “Coordinated beamforming with artificial noise for secure swipt under non-linear eh model: Centralized and distributed designs,” IEEE Journal on Selected Areas in Communications, vol. 36, no. 7, pp. 1544–1563, 2018.
[45] L. E. Dubins and D. A. Freedman, “Machiavelli and the gale-shapley algorithm,” The American Mathematical Monthly, vol. 88, no. 7, pp. 485–494, 1981.
[46] W. Lu, K. An, and T. Liang, “Robust beamforming design for sum secrecy rate maximization in multibeam satellite systems,” IEEE Transactions on Aerospace and Electronic Systems, vol. 55, no. 3, pp. 1568–1572, 2019.
[47] Y. Nesterov, “Semidefinite relaxation and nonconvex quadratic optimization,” Optimization methods and software, vol. 9, no. 1-3, pp. 141–160, 1998.
[48] M. Grant and S. Boyd, “Cvx: Matlab software for disciplined convex programming, version 2.1,” 2014.
[49] N. D. Sidiropoulos, T. N. Davidson, and Z.-Q. Luo, “Transmit beamforming for physical-layer multicasting,” IEEE transactions on signal processing, vol. 54, no. 6, pp. 2239–2251, 2006.
[50] Z.-Q. Luo, W.-K. Ma, A. M.-C. So, Y. Ye, and S. Zhang, “Semidefinite relaxation of quadratic optimization problems,” IEEE Signal Processing Magazine, vol. 27, no. 3, pp. 20–34, 2010.
[51] H. U. Sokun, E. Bedeer, R. H. Gohary, and H. Yanikomeroglu, “Optimization of discrete power and resource block allocation for achieving maximum energy efficiency in ofdma networks,” IEEE Access, vol. 5, pp. 8648–8658, 2017.
[52] F. Bai, N. Sadagopan, and A. Helmy, “Important: A framework to systematically analyze the impact of mobility on performance of routing protocols for adhoc networks,” in IEEE INFOCOM 2003. Twenty-second Annual Joint Conference of the IEEE Computer and Communications Societies (IEEE Cat. No. 03CH37428), vol. 2. IEEE, 2003, pp. 825–835.
[53] X. Lin, R. K. Ganti, P. J. Fleming, and J. G. Andrews, “Towards understanding the fundamentals of mobility in cellular networks,” IEEE Transactions on Wireless Communications, vol. 12, no. 4, pp. 1686–1698, 2013.